

# Efficient implementation of quantum signal processing via the adiabatic-impulse model

D. O. Shendryk,<sup>1,2,\*</sup> O. V. Ivakhnenko,<sup>1,3,\*</sup> S. N. Shevchenko,<sup>1,†</sup> and Franco Neri<sup>3,4</sup>

<sup>1</sup>*B. Verkin Institute for Low Temperature Physics and Engineering, Kharkiv 61103, Ukraine*

<sup>2</sup>*Ruhr-Universität Bochum 44780, Germany*

<sup>3</sup>*Quantum Computing Center, RIKEN, Wakoshi, Saitama, 351-0198, Japan*

<sup>4</sup>*Physics Department, The University of Michigan, Ann Arbor, MI 48109-1040, USA*

Here we investigate analogy between quantum signal processing (QSP) and the adiabatic-impulse model (AIM) in order to implement the QSP algorithm with fast quantum logic gates. QSP is an algorithm that uses single-qubit dynamics to perform a polynomial function transformation. AIM effectively describes the evolution of a two-level quantum system under strong external driving field. We can map parameters from QSP to AIM to implement QSP-like evolution with non-adiabatic, high-amplitude external drives. By choosing AIM parameters that control non-adiabatic transition parameters (such as driving amplitude  $A$ , frequency  $\omega$ , and signal timing), one can achieve polynomial approximations and increase robustness in quantum circuits. The analogy presented here between QSP and AIM can be useful as a way to directly implement the QSP algorithm on quantum systems and obtain all the benefits from the fast Landau-Zener-Stückelberg-Majorana (LZSM) quantum logic gates.

## I. INTRODUCTION

Quantum algorithms represent an innovative paradigm in computational science, using the principles of superposition, entanglement, and quantum interference to confront overwhelmingly time-consuming problems for classical approaches. Beyond the standard narratives of quantum speedup, quantum algorithms challenge assumptions in complexity theory by redefining the boundaries of efficiently solvable problems, such as Hamiltonian simulation, quantum search, quantum factoring, and quantum walks [1–7].

Quantum Signal Processing (QSP) is one such algorithm exploiting single-qubit dynamics with interference, enabling polynomial function transformations with  $O(d)$  elementary unitary operations on the quantum subsystem, where  $d$  is the degree of the polynomial function [8]. QSP algorithms have already undergone several improvements, leading to the development of new algorithms based on it, that enhance performance, address QSP problems [9] and can also be used as a part of more complex algorithms such as quantum search, Hamiltonian simulation, quantum phase estimation, etc. [5, 8]. QSP involves a combination of adjustable rotations around the  $z$ -axis, which produce phase differences between energy levels, and fixed  $x$ -axis rotations on the Bloch sphere, which change the energy levels occupation. These  $x$ - and  $z$ -axes rotations are applied one by one in a sequence. Such QSP sequences of pulses can be used as a component of a composite pulse approach that allows to increase robustness to driving signal noise [10].

We found that the combination of consecutive rotations around the  $x$ - and  $z$ -axes is also directly described by the so-called adiabatic-impulse model (AIM) [11],

a model specifically developed for non-adiabatic single-qubit quantum dynamics, with particular emphasis on interferometry [12, 13]. It is a useful tool to investigate analytically the dynamics of quantum systems with a small energy gap [13, 14]. It combines adiabatic evolution, where the energy levels occupation is conserved but a phase difference is gained, and diabatic (impulse-type) transitions, during which the interference of the amplitudes of different states occurs. Thus, AIM results in a combination of rotations around the  $x$ - and  $z$ -axes, as in QSP. We find it beneficial to explore the analogy between the two approaches—QSP and AIM—and demonstrate that parameters obtained from AIM can be used to effectively implement QSP.

The rest of the paper is organized as follows. In Sec. II, we review the key notions of the work: QSP and AIM. In Sec. III, we describe the algorithms for converting parameters from QSP to AIM. In Sec. IV, we show the way to use two Landau-Zener-Stückelberg-Majorana (LZSM) transitions [12, 13, 15] to implement QSP with reduced duration. In addition, we show an analogy between double LZSM transitions and a Mach-Zehnder interferometer to implement a rotation operator around the  $x$ -axis by an arbitrary angle.

## II. REVIEW OF QUANTUM SIGNAL PROCESSING AND ADIABATIC-IMPULSE MODEL

### A. Quantum Signal Processing

Quantum Signal Processing is a quantum algorithm initially designed for implementing polynomial transformations of matrix eigenvalues via phase modulation [6], originally developed for nuclear magnetic resonance applications [16]. It can also be used to enhance signal sensitivity to specific input parameters, making it a powerful tool for error mitigation, quantum optimization, and

\* These authors contributed equally

† [sshevchenko@ilt.kharkov.ua](mailto:sshevchenko@ilt.kharkov.ua)

quantum machine learning tasks [17, 18]. For instance, the algorithm can be applied to amplify weak signals beyond the limits of repetition statistics and suppress noise without direct measurement [16].

The QSP algorithm involves using a sequence of unitary rotations of a qubit state on the Bloch sphere around the  $x$ - and  $z$ -axes. The operator responsible for rotations around the  $x$ -axis is denoted as the *signal rotation operator*  $W$ , and the operator responsible for rotation around the  $z$ -axis is called the *signal processing operator*  $S$

$$\begin{aligned} W(a) &= \exp\left(i\frac{\theta(a)}{2}X\right) = \begin{pmatrix} a & i\sqrt{1-a^2} \\ i\sqrt{1-a^2} & a \end{pmatrix}, \\ S(\phi) &= \exp(i\phi Z), \end{aligned} \quad (1)$$

where  $X$  and  $Z$  stand for the Pauli matrices  $\sigma_x$  and  $\sigma_z$ , respectively. Here the parameter  $a$  is defined as

$$a = \cos(\theta/2) \in [-1, 1]. \quad (2)$$

For a set of phases

$$\Phi = (\phi_0, \phi_1, \dots, \phi_d), \quad (3)$$

the operator  $U$ , which represents the evolution in the QSP algorithm, is defined as the sequential application of the signal processing operator  $S$  and the signal rotation operator  $W$ :

$$U_{\Phi,a} = \exp(i\phi_0 Z) \prod_{k=1}^d W(a) \exp(i\phi_k Z) \in SU(2). \quad (4)$$

Therefore, the operators  $W$  and  $S$  can be written in the following way using rotation operators

$$W(a(\theta)) = R_x(-\theta), \quad S(\phi) = R_z(-2\phi). \quad (5)$$

Quantum rotation gates  $R_x$  and  $R_z$  describe rotations of single-qubit states on the Bloch sphere by angles  $\alpha$  and  $\beta$  around the  $x$ - and  $z$ -axes, respectively. These gates are defined both in terms of matrix exponentials and explicit matrix representations

$$R_x(\alpha) = \exp\left(-i\frac{\alpha}{2}X\right) = \begin{pmatrix} \cos\left(\frac{\alpha}{2}\right) & -i\sin\left(\frac{\alpha}{2}\right) \\ -i\sin\left(\frac{\alpha}{2}\right) & \cos\left(\frac{\alpha}{2}\right) \end{pmatrix}, \quad (6a)$$

$$R_z(\beta) = \exp\left(-i\frac{\beta}{2}Z\right) = \begin{pmatrix} \exp(-i\frac{\beta}{2}) & 0 \\ 0 & \exp(i\frac{\beta}{2}) \end{pmatrix}. \quad (6b)$$

The equation (4) can be written in terms of rotation operators  $R_x$  and  $R_z$

$$U_{\Phi,a} = R_z(-2\phi_0) \prod_{k=1}^d R_x(-\theta) R_z(-2\phi_d). \quad (7)$$

One of the most remarkable properties of the QSP framework is its ability to construct quantum circuits that

implement a desired polynomial transformation on the eigenvalues of an operator. The inverse of this principle is also true: given a target polynomial  $M(a)$ , there exists a corresponding set of QSP phase angles  $\Phi$  such that the transformation  $M(a)$  can be exactly represented as  $\langle 0|U_{\Phi,a}|0\rangle$ . This principle is formalized in Theorem 1 (Quantum Signal Processing) of Ref. [8], which states that the QSP sequence  $U_{\Phi,a}$  generates a matrix elements, expressible via polynomial function of  $a$ :

$$U_{\Phi,a} = \begin{pmatrix} M(a) & iQ(a)\sqrt{1-a^2} \\ iQ^*(a)\sqrt{1-a^2} & M^*(a) \end{pmatrix}. \quad (8)$$

For this construction to hold, the polynomials  $M(a)$  and  $Q(a)$  must satisfy several conditions. The degree of the polynomial  $M(a)$  must be at most  $d$  and the degree of  $Q(a)$  must be at most  $(d-1)$ . The polynomials must also exhibit parity relationships with the degree  $d$ , and a normalization condition must ensure the unitarity of the resulting transformation. Moreover, for any polynomials  $M(a)$  and  $Q(a)$  satisfying the feasibility conditions, such a sequence of phase angles  $\Phi$  always exists.

As an example, we now consider how Chebyshev polynomials  $T_d(a)$  [19] naturally arise within the framework of QSP [8] and enable polynomial transformations. For trivial phase sequences (i.e., all phases in  $\Phi$  are zero), the resulting polynomials  $M(a)$  align exactly with  $T_d(a)$ :

- For  $\Phi = (0, 0)$ , the corresponding polynomial is
$$M(a) = a = T_1(a); \quad (9a)$$

- For  $\Phi = (0, 0, 0)$ , the polynomial becomes
$$M(a) = 2a^2 - 1 = T_2(a); \quad (9b)$$

- For  $\Phi = (0, 0, 0, 0)$ , the result is
$$M(a) = 4a^3 - 3a = T_3(a). \quad (9c)$$

These results demonstrate that QSP can directly generate the Chebyshev polynomials, which are defined recursively as

$$T_0(a) = 1, \quad T_1(a) = a; \quad (10a)$$

$$T_d(a) = 2aT_{d-1}(a) - T_{d-2}(a) = \cos(d \arccos a). \quad (10b)$$

Another important QSP sequence is BB1 (Broadband 1) [16]. It is a robust composite pulse sequence used in NMR to correct amplitude errors in RF pulses. It is particularly useful for achieving high-fidelity spin manipulations, even when the RF field strength is not perfectly calibrated. To perform the BB1 sequence, we use

$$\Phi = (\pi/2, -\eta, 2\eta, 0, -2\eta, \eta), \quad (11)$$

$$\text{where } \eta = \frac{1}{2} \cos^{-1}(-1/4),$$

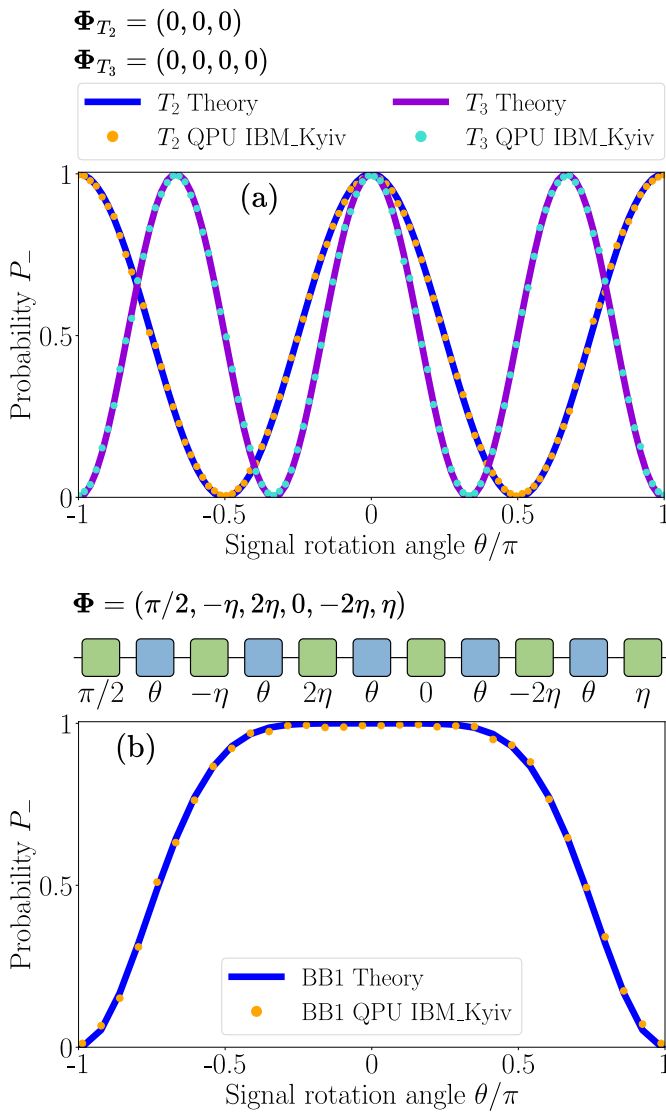


FIG. 1. Occupation probability  $P_-$  after the QSP sequence applied to the qubit with ground state initial conditions. Chebyshev polynomials with Eqs. (9b,9c) are shown in panel (a). The BB1 sequence, corresponding to the polynomial in Eq. (12), is shown in panel (b) (solid curves). Orange dots correspond to the probability obtained by performing the respective QSP sequences on an IBM-Q quantum processing unit (QPU). The scheme for the BB1 sequence is shown in terms of QSP operators, where green boxes correspond to the signal processing operator  $S(\phi)$  and blue boxes correspond to the signal rotation operator  $W(a)$ .

which results in the polynomial:

$$M(a) = \frac{1}{8}a^2 [3a^8 - 15a^6 + 35a^4 - 45a^2 + 30]. \quad (12)$$

The BB1 sequence describes a qubit that remains in the excited state in the broad region  $\theta \approx (-2/3\pi, 2/3\pi)$ , and quickly becomes flipped out of it.

In Fig. 1 we illustrate the resulting probability after applying the QSP sequence with the trivial sequences for

the Chebyshev polynomials in panel (a) and BB1 phase sequence in panel (b). A comparison is made between these results and those obtained from running the corresponding QSP sequences on a quantum computer via IBM-Q cloud quantum computing on the QPU based on the IBM Eagle r3 architecture [20]. We obtained good agreement for this simple single-qubit algorithm despite dissipative and noisy environment of the real qubits in the IBM-Q processor.

The unitary operator  $U_{\Phi,a}$  can then be used in quantum simulations [5, 8] to address computational or physical problems. In general, by varying the number of phases and their configurations using the QSP method [8], it is possible to construct any symmetric signal profile sensitive to the desired combinations of rotation angles.

Later, in Sec. III, we demonstrate how closely this algorithm resembles the adiabatic-impulse model.

## B. Adiabatic-impulse model

The adiabatic-impulse model [11, 21–25] describes the evolution of a system driven by a periodic signal with a linear transition through anti-crossing point (point of the minimal energy gap). This model works well with systems with small energy gap and can be used as a basis for quantum logic gates [14, 26–28]. The evolution is divided into two regimes: the adiabatic regime, where the system closely follows its adiabatic states, and the diabatic impulse-type regime, where a transition of occupation probability between two energy levels occurs, accompanied by a phase gain between different energy level occupations.

First, we consider a typical qubit Hamiltonian

$$H = \frac{\Delta}{2}X + \frac{\varepsilon(t)}{2}Z, \quad (13)$$

where  $\Delta$  is the minimal energy gap between the two energy levels and  $\varepsilon(t) = -A \cos \omega t$  is the driving signal with frequency  $\omega$  and large amplitude  $A > \Delta$ . The evolution is separated into adiabatic evolution, described by the matrix  $U$ , and transition (impulse-type) evolution described, by the matrix  $N$ :

$$U(t_i, t_j) = \begin{pmatrix} \exp(-i\zeta(t_i, t_j)) & 0 \\ 0 & \exp(i\zeta(t_i, t_j)) \end{pmatrix} \quad (14a)$$

$$= \exp(-i\zeta Z) = R_z(2\zeta),$$

$$N = \begin{pmatrix} \mathcal{R}e^{-i\phi_S} & -\mathcal{T} \\ \mathcal{T} & \mathcal{R}e^{i\phi_S} \end{pmatrix} = R_z(\phi_S)R_x(\theta)R_z(\phi_S), \quad (14b)$$

$$\phi_S = \frac{\pi}{4} + \delta(\ln \delta - 1) + \arg[\Gamma(1 - i\delta)], \quad \delta = \frac{\Delta^2}{4\hbar v},$$

$$\mathcal{T} = \sqrt{\mathcal{P}}, \quad \mathcal{R} = \sqrt{1 - \mathcal{P}}, \quad \mathcal{P} = \exp\left[\frac{-\pi\Delta^2}{2A\hbar\omega}\right]. \quad (14c)$$

where  $\phi_S$  is the Stokes phase,  $v = \left.\frac{d\varepsilon(t)}{dt}\right|_{\varepsilon=0} = A\omega$  is the speed of the anti-crossing passage (first derivative of the driving signal in the anti-crossing point),  $\mathcal{T}$  is

the transmission coefficient that is equivalent to  $a$  in the QSP algorithm, so that the polynomial base in QSP is the transmission coefficient. Moreover  $\mathcal{R}$  is the reflection coefficient,  $\mathcal{P}$  is the LZSM excitation probability of the qubit with a single transition from the ground state [29–35], and  $\delta$  is the adiabaticity parameter. Note that the transition matrix  $N$  depends on the direction of the crossing of the anti-crossing region and in the case of inverse crossing, the matrix  $N^{\text{inv}}$  includes an additional phase  $\pi$  along with the Stokes phase [13, 24], or in other words it equals to the transposed transition matrix  $N^{\text{inv}} = N^\top$ . The phase, accumulated during the adiabatic evolution of the system, is:

$$\zeta(t_i, t_j) = \frac{1}{2\hbar} \int_{t_i}^{t_j} \Delta E(t) dt, \quad (15a)$$

$$\Delta E(t) = \sqrt{\varepsilon(t)^2 + \Delta^2}. \quad (15b)$$

According to the AIM, the evolution of the system is adiabatic everywhere except at the LZSM transition point (or anti-crossing point), while the transition itself is considered instantaneous in the AIM, and the evolution during this time is described as diabatic. In this case, the complete evolution of the system during a single LZSM transition, from the initial state  $\psi_{\text{in}}$  (index 1) to the final state  $\psi_{\text{fin}}$  (index 2) consists of adiabatic evolution before the anti-crossing point, transition evolution at the anti-crossing point, and adiabatic evolution after the anti-crossing point:

$$U_{\text{LZSM}} = U(\zeta_2) N U(\zeta_1) = \begin{pmatrix} U_{11} & U_{12} \\ -U_{12}^* & U_{11}^* \end{pmatrix}, \quad (16)$$

$$U_{11} = \mathcal{R}_1 \exp[-i(\phi_S + \zeta_1 + \zeta_2)],$$

$$U_{12} = -\mathcal{T}_1 \exp[i(\zeta_1 - \zeta_2)],$$

where  $\zeta_1$  and  $\zeta_2$  are the *phase gains* before and after the anti-crossing point, respectively.

The complete evolution matrix for a single transition in terms of Bloch sphere rotation operators is

$$U_{\text{LZSM}_{1 \rightarrow 2}} = R_z(2\zeta_2 + \phi_S) R_x(\theta) R_z(2\zeta_1 + \phi_S). \quad (17)$$

The principal structure of the AIM evolution in Eq. (17) is identical to that of the QSP in Eq. (7), differing only in parameter values that can be tuned as needed.

### III. AN ALGORITHM FOR CONVERTING QSP PARAMETERS TO AIM

Here, we present a method for aligning the phases of the QSP sequence with those in AIM. We develop an algorithm to adapt QSP phases for AIM, which provides the experimental inputs—amplitude, frequency, and timings—needed for the direct realization of the QSP sequence on an experimental device with LZSM-type evolution, using the method of determining parameters from AIM [14].

We now consider a harmonic signal that is linear in the vicinity of the anti-crossing region, meaning it corresponds to analytical solutions for the probability of an LZSM transition and results in the LZSM transition probability. From Eq. (14c) we have

$$\left. \frac{d\varepsilon}{dt} \right|_{\varepsilon=0} = A\omega = \frac{-\pi\Delta^2}{2\hbar \ln \mathcal{P}}. \quad (18)$$

The total phase gain during the LZSM transition is called the Stückelberg phase and it is expressed as the sum of the Stokes phase  $\phi_S$  given by the Eq. (14b), gained during diabatic evolution, and the phase accumulated during the adiabatic evolution of the system  $\zeta(t_i, t_j)$  given by Eq. (15a)

$$\phi_{\text{St}} = \phi_S + \zeta(t_i, t_j). \quad (19)$$

The steps for determining the amplitude  $A$ , frequency  $\omega$ , and time  $\Delta t = t_j - t_i$  for a driven signal with a LZSM transition can be described as follows:

1. Given that the system undergoes a rotation by an angle  $\theta$  about the  $x$ -axis, the probability of finding the system in the upper state after a single LZSM transition can be found from the following equation:

$$\mathcal{P} = \sin^2(\theta/2). \quad (20)$$

Next, since we start and finish the transition far from the anti-crossing point, we fix the amplitude to ensure that the next transition starts from the same detuning  $\varepsilon$  as when we finish the previous one. Using the previously defined LZSM probability in Eq. (14c), we obtain the driving frequency:

$$\omega = \frac{-\pi\Delta^2}{2\hbar A \ln \mathcal{P}}. \quad (21)$$

2. The phase correspondence condition can be found by comparing the evolution matrices for a two-level system described by AIM in Eqs. (14a, 14b, 16) and the one for QSP with corresponding QSP phases in Eq. (4):

$$\begin{aligned} U_{\Phi, a} &= \exp(i\phi_0 Z) \prod_{k=1}^d W(a) \exp(i\phi_k Z) \\ &= R_z(-2\phi_0) \prod_{k=1}^d R_x(-\theta) R_z(-2\phi_k). \end{aligned} \quad (22)$$

3. We use a signal, shown in Fig. 2 and defined as,

$$\varepsilon(t) = \begin{cases} A, & \text{if } t < T_s, \\ -A \cos(\omega(t - T_s)), & \text{if } T_s \leq t < T_s + \frac{\pi}{\omega}, \\ -A, & \text{if } t \geq T_s + \frac{\pi}{\omega}, \end{cases} \quad (23)$$

where  $T_s$  is the time needed to accumulate the correct phase gain before the transition, because we use a symmetrical driving signal.

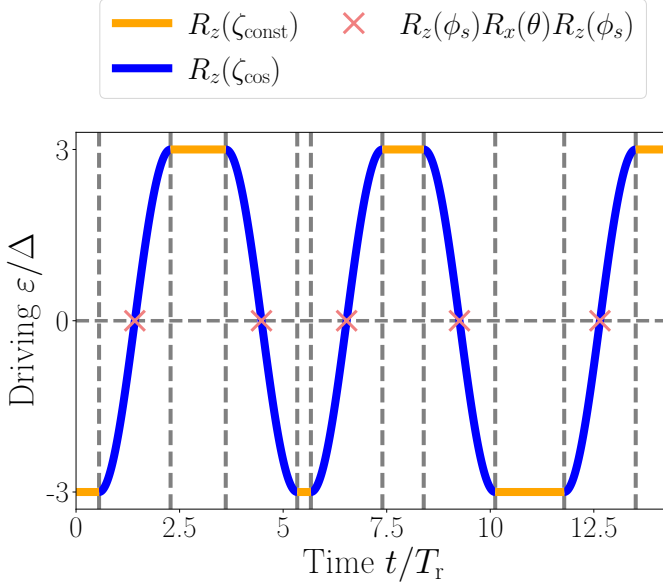


FIG. 2. Signal shape for the BB1 sequence realized with AIM. We assumed large amplitude,  $A = 3\Delta$ . The blue line corresponds to the harmonic driven evolution described by the cosine in Eq. (23), the orange line corresponds to the adjustable phase gain while the driving is constant, which is used to match the QSP phases with the AIM phases, and the red crosses are the transition points. Time is normalized to the qubit resonant excitation period  $T_r$ .

According to Step 2, for  $d$  LZSM transitions, the mapping of AIM phases to QSP is determined by the following phase relations:

$$\begin{aligned}
 \phi_S + 2\zeta_{\text{const},0}(t) + 2\zeta_{\text{cos}}(t) + 2\pi j &= -2\phi_0, \\
 2\phi_S + 2\zeta_{\text{const},1}(t) + 2\zeta_{\text{cos}}(t) + \pi + 2\pi j &= -2\phi_1, \\
 \dots & \\
 2\phi_S + 2\zeta_{\text{const},d-1}(t) + 2\zeta_{\text{cos}}(t) + \pi + 2\pi j &= -2\phi_{d-1}, \\
 \phi_S + 2\zeta_{\text{const},d}(t) + 2\zeta_{\text{cos}}(t) + \pi + 2\pi j &= -2\phi_d, \quad d \text{ is even,} \\
 \phi_S + 2\zeta_{\text{const},d}(t) + 2\zeta_{\text{cos}}(t) + 2\pi j &= -2\phi_d, \quad d \text{ is odd,}
 \end{aligned} \tag{24}$$

here  $j$  is an integer and  $k = 0, 1, \dots, d$ ,

$$\zeta_{\text{const},k} = \Omega_L T_{\text{const},k}/2, \quad \Omega_L = \sqrt{A^2 + \Delta^2}/\hbar, \tag{25a}$$

$$\zeta_{\text{cos}} = \frac{1}{2\hbar} \int_0^{T_{\text{cos}}/2} \sqrt{A^2 \cos^2(\omega(t - T_s)) + \Delta^2} dt, \tag{25b}$$

where  $T_{\text{const},k}$  is the duration of the free evolution stage,  $T_{\text{cos}} = 2\pi/\omega$  is the period of the resonance driving. Note that free evolution precession around the  $z$ -axis happen with the Larmor frequency  $\Omega_L$  and period  $T_L = 2\pi/\Omega_L$ . In these conditions, the phases  $\zeta_{\text{const}}$  and  $\zeta_{\text{cos}}$  are gained during the free-evolution stage, where  $\varepsilon = \pm A$ , and during the LZSM transition, where  $\varepsilon = \pm A \cos(\omega t)$ , respectively. After determining the target phases  $\Phi = (\phi_0, \phi_1, \dots, \phi_d)$ , the evolution time is obtained to satisfy the conditions in Eq. (24) and achieve the target QSP parameters mentioned above.

In this section we demonstrate the direct implementation of the QSP algorithm evolution using AIM. The execution time of the operations is determined by the LZSM probability in Eq. (14c), which corresponds to the rotation angle around the  $x$ -axis on the Bloch sphere and the chosen amplitude of the driving signal  $A$ . Notably, for specific values of the LZSM probability  $\mathcal{P} = 0$ , the operation time  $T_{\text{cos}} = 2\pi/\omega$ , see Eq. (21), diverges to infinity. The next section is devoted to a way how to resolve this problem.

#### IV. DOUBLE LANDAU-ZENER-STÜCKELBERG-MAJORANA TRANSITION QUANTUM SIGNAL PROCESSING ALGORITHM

Here we describe how to use double LZSM transitions [14] for realizing QSP. Double LZSM transitions allow eliminating the huge time variability of each QSP rotation around the  $x$ -axis. A double LZSM transition is fully equivalent to a Mach-Zehnder interferometer with two beam splitters (LZSM transitions) with a phase gain between beam splitters or LZSM transitions and interferometry between states [13, 36, 37] (adiabatic evolution). Here we use  $\mathcal{P} = 0.5$ , which is equivalent to a (commonly used in photonics) 50/50 beam splitter.

In particular, the Mach-Zehnder interferometer in photonic quantum computers is used as a *programmable quantum gate*, programmed by adjusting the phase gain between beam splitters [38–40]. To adjust the rotation angle of the signal rotation operator  $W$ , we use adjustable additional free evolution between two LZSM transitions. For a double LZSM transition [14] with adjustable phase gain between two transitions, we have

$$\begin{aligned}
 \Xi &= U_1 N_2 U_1 U_2 N_1^{\text{inv}} U_2 \\
 &= U_{\text{LZSM}(1)}^{\text{inv}} U_{\text{LZSM}(2)} = \begin{pmatrix} \Xi_{11} & \Xi_{12} \\ -\Xi_{12}^* & \Xi_{11}^* \end{pmatrix}, \tag{26}
 \end{aligned}$$

where for the adiabatic evolution between transitions we use  $U_2$  with an adjustable phase,  $U_2 = U(\zeta_2 + \phi_{\text{ad}})$ ,  $\phi_{\text{ad}}$  is an additional phase gain between two LZSM transitions. For the Stückelberg phase  $\phi_{\text{St}} = \phi_S + \zeta_2$ , we choose conditions for the X gate from Ref. [14],  $\phi_{\text{St}} = \frac{\pi}{2}$ ,  $\mathcal{R} = \mathcal{T} = \frac{1}{\sqrt{2}}$ . Then we obtain

$$\Xi_{11} = [\mathcal{R}^2 \exp(-i(2\phi_S + 2\zeta_2 + 2\phi_{\text{ad}})) + \mathcal{T}^2] \cdot \exp[i(\phi_{\text{ad}} + \zeta_2 - \phi_{\text{in}} - \zeta_1 - \phi_{\text{fin}} - \zeta_3)], \tag{27}$$

$$\Xi_{12} = \mathcal{R}\mathcal{T}[1 - \exp(-i(2\phi_S + 2\zeta_2 + 2\phi_{\text{ad}}))] \cdot \exp[i(\phi_S + \phi_{\text{ad}} + \zeta_2 + \phi_{\text{in}} + \zeta_1 - \phi_{\text{fin}} - \zeta_3)], \tag{28}$$

where

$$\begin{aligned}
 \zeta_1 &= \zeta(0, t_{S1}), \\
 \zeta_2 + \phi_{\text{ad}} &= \zeta(t_{S1}, t_{S2}), \\
 \zeta_3 &= \zeta(t_{S2}, t_{\text{final}}).
 \end{aligned} \tag{29}$$

We use a symmetric harmonic signal to perform LZSM transitions, such that  $\zeta_2 = \zeta_1 + \zeta_3$  and  $\zeta_1 = \zeta_3$ . Additionally, we have a phase gain before the transition  $\phi_{\text{in}}$  and after the transition  $\phi_{\text{fin}}$ , where  $t_{S1,2}$  represent the times at which the first and second LZSM transition signals start within the double LZSM transition (each transition signal is half period of the harmonic signal), and  $t_{\text{final}}$  is the final time of the second LZSM transition.

Next, to obtain the parameters for rotation around the  $x$ -axis on a Bloch sphere, we compare the double LZSM transition matrix elements with the respective ones for a rotation operator around the  $x$ -axis on a Bloch sphere  $R_x(\theta)$

$$R_x(\theta)_{11} = \cos \theta/2, \quad (30a)$$

$$R_x(\theta)_{12} = -i \sin \theta/2. \quad (30b)$$

Then to obtain the phases, necessary to perform the  $R_x$  gate, we solve the corresponding system of equations  $\Xi = R_x(\theta)$ :

$$\begin{cases} \cos \frac{\theta}{2} = \frac{1}{2} (1 + e^{-i(\pi+2\phi_{\text{ad}})}) e^{i(\phi_{\text{ad}}-\phi_{\text{in}}-\phi_{\text{fin}})} \\ e^{i3\pi/2} \sin \frac{\theta}{2} = \frac{1}{2} (1 - e^{-i(\pi+2\phi_{\text{ad}})}) e^{i(\phi_{\text{ad}}+\phi_{\text{in}}-\phi_{\text{fin}}+\pi/2)} \end{cases}. \quad (31)$$

As a result, by using Euler's formula for cosine and sine, we obtain a system of equations for the phases. By solving this system of equations, we obtain additional phases to perform the  $R_x(\theta)$  operation for the same LZSM driving parameters as for the  $X$  gate in Ref. [14]

$$\begin{cases} \phi_{\text{in}} = \pi/4 + 2\pi n, \\ \phi_{\text{fin}} = 5\pi/4 + 2\pi n, \\ \phi_{\text{ad}} = \theta/2 + \pi/2 + \pi n. \end{cases} \quad (32)$$

The minimum time of free evolution is equal to the fractional part of the phase divided by  $2\pi$  and multiplied by the period of the free evolution. Thus, for all additional phases, the waiting time becomes

$$\begin{cases} t_{\text{ad}} = \left\{ \frac{\theta + \pi}{2\pi} \right\} T_L, \\ t_{\text{in}} = \left\{ \frac{\pi/2}{2\pi} \right\} T_L = T_L/4, \\ t_{\text{fin}} = \left\{ \frac{5\pi/2}{2\pi} \right\} T_L = T_L/4. \end{cases} \quad (33)$$

With the driving signal  $\varepsilon(t) = -A \cos \omega t$ , the first transition will be reversed, that lead to an additional  $\pi$  phase to the initial phase gain [14]. This gives the free evolution time that should be added at the beginning of the sequence, denoted as  $t_{\text{in}}$ , and between the signal rotation operators, denoted as  $t_{\text{mid}}$  for the rotation around the  $x$ -axis

$$t_{\text{mid}} = \left\{ \frac{5\pi/2 + \pi/2}{2\pi} \right\} T_L = T_L/2. \quad (34)$$

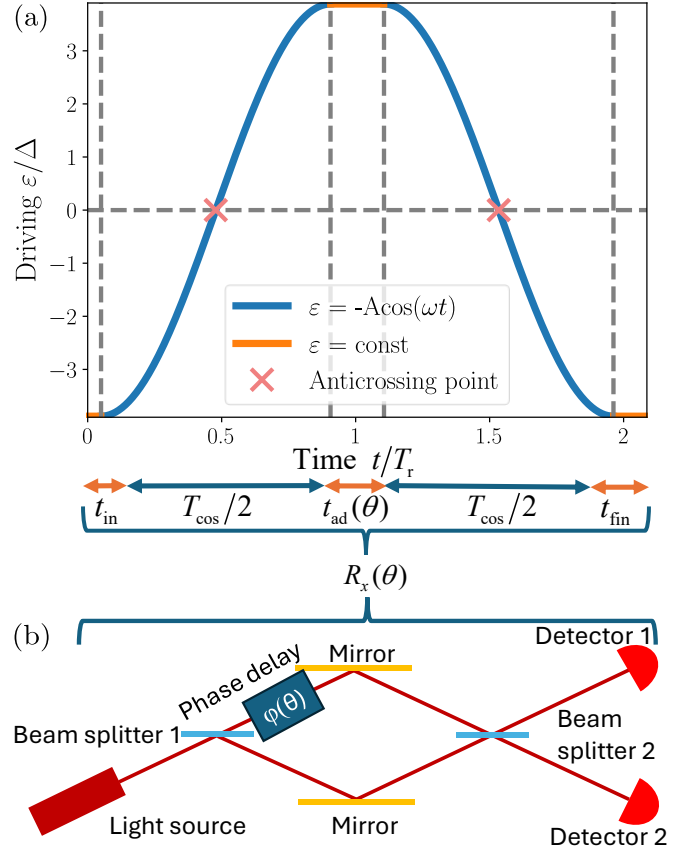


FIG. 3. (a) Adjustable rotation gate  $R_x(\theta)$  with double LZSM transition. (b) Analogy for realizing an  $R_x(\theta)$  rotation gate with a Mach-Zehnder interferometer.

So, we described how to get all the necessary phases such as the phase gain time-intervals before the sequence, between double LZSM transitions, and after the sequence. To get the amplitude and the frequency we use the algorithm, described in Ref. [14] for the  $X$ -gate. With these we have all the parameters required to implement QSP sequences using double LZSM transitions.

Double LZSM transitions allow us to eliminate the main weakness of the direct implementation of the QSP algorithm with AIM: the transition time diverges as the signal rotation angle approaches zero, making the result highly susceptible to decoherence and dissipation. Double transitions allow to perform the QSP sequence fast and with high fidelity by leveraging the LZSM gates technique, using the same driving signal defined for the  $X$ -gate in Ref. [14] with the additional free evolution time between transitions  $t_{\text{ad}}$  for the signal operator  $W = R_x(\theta)$ . Then we perform the signal processing operator  $S = R_z(\phi_i)$  after each transition. By choosing a working point with higher amplitude, we can significantly improve the fidelity of LZSM gates by slightly decreasing the gate execution time.

Figure 3(a) shows the driving signal used to implement the  $R_x(\theta)$  gate, where the time between transitions  $t_{\text{ad}}$

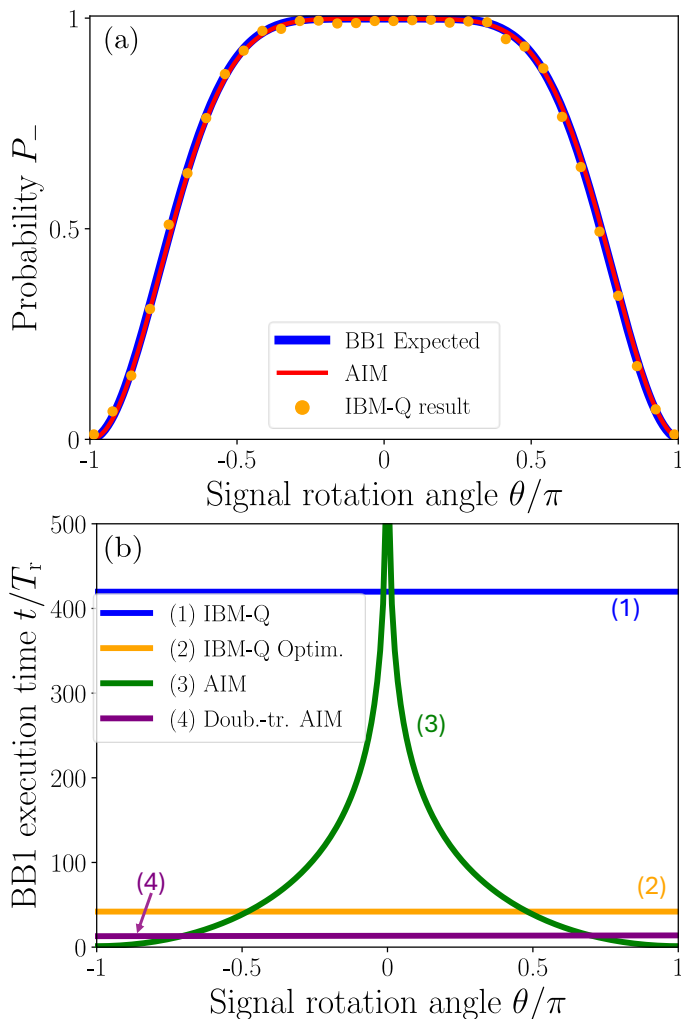


FIG. 4. Panel (a) shows the resulting occupation probability  $P_-$  for the BB1 sequence in Eq. (12) compared to the qubit dynamics simulation result with the driving signal defined by AIM. Panel (b) presents a comparison of the hardware execution time for the BB1 sequence using different approaches: (1) IBM-Q time (blue line), computed as the difference between the execution time with zero gates and the time with the BB1 sequence. This isolates the time required solely for the QSP algorithm, enabling direct comparison with other methods. (2) IBM-Q with the highest optimization setting (orange line), where the execution time does not depend on the number of single-qubit gates—i.e., the entire BB1 sequence is replaced with a single compiled gate. (3) Direct realization of QSP via AIM (green curve). (4) Double LZSM transitions (purple line). To compare times we divide all of them by the period of the resonance driving  $T_r = 2\pi/\Delta$ .

(upper panel) is defined by the rotation angle around the  $x$ -axis, and the time intervals  $t_{\text{in}}$  and  $t_{\text{fin}}$  are used to gain additional phases before and after transitions to perfectly match our double LZSM transition matrix to an  $R_x(\theta)$  gate.

Figure 3(b) shows the equivalent Mach-Zehnder interferometer scheme which is used as a programmable

quantum logic gate for photons, where the rotation angle around the  $x$ -axis is defined by additional phase gain in one of the optical ways of the Mach-Zehnder interferometer, that can be tunable.

## V. EXECUTION TIME OF THE QSP ALGORITHM

Figure 4(a) shows a comparison of the excitation probability after applying the BB1 sequence. The IBM-Q result is shown by orange dots. Qubit dynamics simulations performed with QuTiP [41–43] (including relaxation and dephasing), for signals defined by AIM using both direct QSP analogy and double LZSM transitions are shown by the red curve. All results show good agreement with the expected polynomial distribution shown by the blue curve.

In Fig. 4(b) we compare the time needed to perform the BB1 sequence by different methods. Note that for the angle  $\theta = 0$  in the QSP algorithm, with direct QSP to AIM analogy, time tends to infinity, as discussed before. This divergence arises due to the definition of the driving frequency in Eq. (21) and the probability of the LZSM transition Eq. (14c), which yields  $\omega = 0$ , so the period of the driving tends to infinity in this case. Note also that the BB1 execution time by the double LZSM transitions results in a stable operation time for all angles  $\theta$ .

We found that the IBM-Q, cloud based quantum computer, needed significantly more time to execute the BB1 sequence, especially for the non-optimized version, where the dependence on the number of gates appears. This is mainly due to the Rabi-like resonance pulse type of the driving used in current quantum computers, which loses fidelity significantly with faster gates. Despite the much faster gate execution time of the optimized algorithm with maximum optimization on an IBM-Q (where the sequence of all single-qubit gates is replaced by just one gate), the double LZSM transition is still several times faster. But the LZSM transitions require a small energy gap in the anti-crossing point and the distance between levels should grow fast with detuning  $\varepsilon$ . Therefore, the speed advantage of the LZSM-based gates may be constrained by hardware limitations in practical implementations.

## VI. CONCLUSIONS

Quantum signal processing is a powerful tool for implementing polynomial transformations and other quantum algorithms with high precision. Due to its structural similarity to the adiabatic-impulse model, it is possible to establish a direct mapping between the parameters of these two approaches, enabling efficient translation of one algorithm into the other. This analogy provides a novel perspective for the direct implementation of QSP in quantum systems.

Furthermore, the use of adiabatic-impulse model, with double Landau-Zener-Stückelberg-Majorana transitions, demonstrates significantly reduced time for implementing quantum signal processing algorithm. The double LZSM transitions allow us to solve the infinite transition time problem for  $\mathcal{P} = 0$  in the direct implementation of QSP with AIM.

The double LZSM transitions approach is a full analog of the Mach-Zehnder interferometer, which allows to use the double transition approach from AIM in a programmable quantum gate for quantum photonic computations [38–40], so the same approaches can be used for both of them. With the double LZSM transition, we show how to perform rotations around the  $x$ -axis on the Bloch sphere for any desired angle  $\theta$ . By combining this with idling times to perform signal processing operators, we can use fast nonadiabatic LZSM gates to perform any QSP sequence and achieving faster execution time even for the most optimized case for the IBM-Q, where all single-qubit gates are combined into one. In principle,

the same single-qubit gate sequence combination technique can be applied for LZSM gates to reduce the execution time accordingly.

The adiabatic-impulse model describes well the dynamics of systems with small energy gaps and can be used as an alternative approach to implement fast quantum logic gates and algorithms such as QSP.

## ACKNOWLEDGMENTS

S.N.S. acknowledges support via the Virtual Short-Term Scientist Engagement Fellowship Program for Ukrainian Scientists with Dual-Use Relevant Expertise (STCU, grant # NSEP1030). F.N. is supported in part by: the Japan Science and Technology Agency (JST) [via the CREST Quantum Frontiers program Grant No. JPMJCR24I2, the Quantum Leap Flagship Program (Q-LEAP), and the Moonshot R&D Grant Number JPMJMS2061], and the Office of Naval Research (ONR) Global (via Grant No. N62909-23-1-2074).

- 
- [1] P. W. Shor, *Proceedings of the 35th Annual Symposium on Foundations of Computer Science* (IEEE Press, Los Alamitos, 1994) pp. 124–134.
- [2] L. K. Grover, Fixed-point quantum search, *Phys. Rev. Lett.* **95**, 150501 (2005).
- [3] F. Magniez, A. Nayak, J. Roland, and M. Santha, Search via quantum walk, *SIAM J. Comput.* **40**, 142 (2011).
- [4] T. J. Yoder, G. H. Low, and I. L. Chuang, Fixed-point quantum search with an optimal number of queries, *Phys. Rev. Lett.* **113**, 210501 (2014).
- [5] G. H. Low and I. L. Chuang, Optimal Hamiltonian Simulation by Quantum Signal Processing, *Phys. Rev. Lett.* **118**, 010501 (2017).
- [6] G. H. Low and I. L. Chuang, Hamiltonian Simulation by Qubitization, *Quantum* **3**, 163 (2019).
- [7] B. Li, S. Ahmed, S. Saraogi, N. Lambert, F. Nori, A. Pitchford, and N. Shammah, Pulse-level noisy quantum circuits with QuTiP, *Quantum* **6**, 630 (2022).
- [8] J. M. Martyn, Z. M. Rossi, A. K. Tan, and I. L. Chuang, Grand unification of quantum algorithms, *PRX Quantum* **2**, 040203 (2021).
- [9] D. Motlagh and N. Wiebe, Generalized quantum signal processing, *PRX Quantum* **5**, 020368 (2024).
- [10] D. Bluvstein, H. Levine, G. Semeghini, T. T. Wang, S. Ebadi, M. Kalinowski, A. Keesling, N. Maskara, H. Pichler, M. Greiner, V. Vuletić, and M. D. Lukin, A quantum processor based on coherent transport of entangled atom arrays, *Nature* **604**, 451 (2022).
- [11] B. Damski and W. H. Zurek, Adiabatic-impulse approximation for avoided level crossings: from phase-transition dynamics to Landau-Zener evolutions and back again, *Phys. Rev. A* **73**, 063405 (2006).
- [12] S. N. Shevchenko, S. Ashhab, and F. Nori, Landau-Zener-Stückelberg interferometry, *Phys. Rep.* **492**, 1 (2010).
- [13] O. V. Ivakhnenko, S. N. Shevchenko, and F. Nori, Nonadiabatic Landau-Zener-Stückelberg-Majorana transitions, dynamics, and interference, *Phys. Rep.* **995**, 1–89 (2023).
- [14] A. I. Ryzhov, O. V. Ivakhnenko, S. N. Shevchenko, M. F. Gonzalez-Zalba, and F. Nori, Alternative fast quantum logic gates using nonadiabatic Landau-Zener-Stückelberg-Majorana transitions, *Phys. Rev. Res.* **6**, 033340 (2024).
- [15] E. P. Glasbrenner and W. P. Schleich, The Landau-Zener formula made simple, *J. Phys. B* **56**, 104001 (2023).
- [16] S. Wimperis, Broadband, narrowband, and passband composite pulses for use in advanced NMR experiments, *J. Mag. Res., A* **109**, 221 (1994).
- [17] Y. Kikuchi, C. Mc Keever, L. Coopmans, M. Lubasch, and M. Benedetti, Realization of quantum signal processing on a noisy quantum computer, *npj Quantum Inf.* **9**, 93 (2023).
- [18] H. Liao, D. S. Wang, I. Sitdikov, C. Salcedo, A. Seif, and Z. K. Mineev, Machine learning for practical quantum error mitigation, *Nat. Mach. Int.* **6**, 1478 (2024).
- [19] M. Abramowitz and I. A. Stegun, *Handbook of mathematical functions: with formulas, graphs, and mathematical tables*, Vol. 55 (Courier Corporation, 1965).
- [20] M. AbuGhanem, IBM quantum computers: evolution, performance, and future directions, *J. Supercomp.* **81**, 687 (2025).
- [21] T. Higuchi, C. Heide, K. Ullmann, H. B. Weber, and P. Hommelhoff, Landau-Zener-Stückelberg interferometer on attosecond timescales in graphene, in *Ultrafast Phenomena and Nanophotonics XXII*, edited by M. Betz and A. Y. Elezzabi (SPIE, 2018) p. 34.
- [22] C. Heide, T. Boolakee, T. Higuchi, and P. Hommelhoff, Adiabaticity parameters for the categorization of light-matter interaction: From weak to strong driving, *Phys. Rev. A* **104**, 023103 (2021).

- [23] P. O. Kofman, O. V. Ivakhnenko, S. N. Shevchenko, and F. Nori, Majorana's approach to nonadiabatic transitions validates the adiabatic-impulse approximation, *Sci. Rep.* **13**, 5053 (2023).
- [24] P. O. Kofman, S. N. Shevchenko, and F. Nori, Tuning the initial phase to control the final state of a driven qubit, *Phys. Rev. A* **109**, 022409 (2024).
- [25] V. Reparaz, M. J. Sánchez, M. Gatto, D. Dominguez, and L. Tosi, Landau-Zener-Stückelberg spectroscopy of a fluxonium quantum circuit, *ArXiv*, 2504.21691 (2025).
- [26] D. L. Campbell, Y.-P. Shim, B. Kannan, R. Winik, D. K. Kim, A. Melville, B. M. Niedzielski, J. L. Yoder, C. Tahan, S. Gustavsson, and W. D. Oliver, Universal nonadiabatic control of small-gap superconducting qubits, *Phys. Rev. X* **10**, 041051 (2020).
- [27] J. J. Cáceres, D. Domínguez, and M. J. Sánchez, Fast quantum gates based on Landau-Zener-Stückelberg-Majorana transitions, *Phys. Rev. A* **108**, 052619 (2023).
- [28] F. Kivelä, S. Dogra, and G. S. Paraoanu, Quantum simulation of the pseudo-Hermitian Landau-Zener-Stückelberg-Majorana effect, *Phys. Rev. Research* **6**, 023246 (2024).
- [29] L. D. Landau and E. M. Lifshitz, *Quantum Mechanics: Non-Relativistic Theory*, 2nd ed. (Pergamon Press, Oxford, 1965) Chap. 53, pp. 185–187, Transition under the action of adiabatic perturbation.
- [30] M. S. Child, On the Stückelberg formula for non-adiabatic transitions, *Mol. Phys.* **28**, 495 (1974).
- [31] M. S. Child, *Molecular collision theory* (Courier Corporation, 2014).
- [32] F. Wilczek, Majorana and condensed matter physics, in *The Physics of Ettore Majorana*, edited by S. Esposito (Cambridge Univ. Press, 2014) pp. 279–302.
- [33] E. P. Glasbrenner, Y. Gerdes, S. Varró, and W. P. Schleich, A different perspective on the Landau-Zener dynamics, *ArXiv*, 2404.08466, (2024).
- [34] S. D. Tedo, O. Feulefack, J. Danga, S. Mkam Tchoubiap, R. Keumo Tsiaze, A. Fotue, N. Hounkonnou, and L. Fai, Harmonic driving and dynamic transitions in the Landau-Zener-Stückelberg-Majorana interferometry induced by tunneling flux-driven symmetric transmon qubits, *Reviews in Physics* **13**, 100118 (2025).
- [35] E. P. Glasbrenner, Y. Gerdes, S. Varró, and W. P. Schleich, Hidden facts in Landau-Zener transitions revealed by the Riccati equation, *ArXiv*, 2502.04033, (2025).
- [36] W. D. Oliver, Y. Yu, J. C. Lee, K. K. Berggren, L. S. Levitov, and T. P. Orlando, Mach-Zehnder interferometry in a strongly driven superconducting qubit, *Science* **310**, 1653 (2005).
- [37] M. Kuzmanović, I. Björkman, J. J. McCord, S. Dogra, and G. S. Paraoanu, High-fidelity robust qubit control by phase-modulated pulses, *Phys. Rev. Research* **6**, 013188 (2024).
- [38] W. Bogaerts, D. Pérez, J. Capmany, D. A. B. Miller, J. Poon, D. Englund, F. Morichetti, and A. Melloni, Programmable photonic circuits, *Nature* **586**, 207 (2020).
- [39] M. Dong, M. Zimmermann, D. Heim, H. Choi, G. Clark, A. J. Leenheer, K. J. Palm, A. Witte, D. Dominguez, G. Gilbert, M. Eichenfield, and D. Englund, Programmable photonic integrated meshes for modular generation of optical entanglement links, *npj Quant. Inf.* **9**, 42 (2023).
- [40] C. Heide, P. D. Keathley, and M. F. Kling, Petahertz electronics, *Nat. Rev. Phys.* **6**, 648 (2024).
- [41] J. Johansson, P. Nation, and F. Nori, QuTiP: An open-source Python framework for the dynamics of open quantum systems, *Comput. Phys. Commun.* **183**, 1760–1772 (2012).
- [42] J. Johansson, P. Nation, and F. Nori, QuTiP 2: A Python framework for the dynamics of open quantum systems, *Comput. Phys. Commun.* **184**, 1234 (2013).
- [43] N. Lambert, E. Giguère, P. Menczel, B. Li, P. Hopf, G. Suárez, M. Gali, J. Lishman, R. Gadhvi, R. Agarwal, A. Galicia, N. Shammah, P. Nation, J. R. Johansson, S. Ahmed, S. Cross, A. Pitchford, and F. Nori, QuTiP 5: The quantum toolbox in Python, *ArXiv*, 2412.04705, (2024).